

Superconducting properties of noncentrosymmetric $\text{Nb}_{0.18}\text{Re}_{0.82}$ thin films probed by transport and tunneling experiments

C. Cirillo,^{1,2} G. Carapella,^{1,2} M. Salvato,^{1,3} R. Arpaia,⁴ M. Caputo,^{1,2} and C. Attanasio^{1,2}

¹*CNR-SPIN Salerno, Università degli Studi di Salerno, I-84084 Fisciano (SA), Italy*

²*Dipartimento di Fisica “E.R. Caianiello”, Università degli Studi di Salerno, I-84084 Fisciano (SA), Italy*

³*Dipartimento di Fisica Università di Roma “Tor Vergata”, I-00133 Roma, Italy*

⁴*Quantum Device Physics Laboratory, Department of Microtechnology and Nanoscience, Chalmers University of Technology, SE-41296 Göteborg, Sweden*

(Received 17 June 2016; revised manuscript received 3 August 2016; published 16 September 2016)

Superconducting thin films of the noncentrosymmetric superconductor $\text{Nb}_{0.18}\text{Re}_{0.82}$ were successfully deposited by UHV sputtering technique. X-ray diffraction analysis indicated that the films are polycrystalline, with a preferential $(nn0)$ orientation and the lattice parameter in agreement with the expected single α -Mn cubic phase. A detailed electrical characterization of the samples as a function of the thickness ($3.5 \text{ nm} \leq d \leq 142 \text{ nm}$) was performed both in the normal and in the superconducting states, revealing a well-established superconducting ordering, as well as an estimated value of the upper critical field, $\mu_0 H_{c2}$, comparable with the Pauli limit. Finally, the symmetry of the order parameter was probed by tunneling spectroscopy on $\text{Al}/\text{Al}_2\text{O}_3/\text{Nb}_{0.18}\text{Re}_{0.82}$ heterostructures, which provides evidence for a single s -wave superconducting gap.

DOI: [10.1103/PhysRevB.94.104512](https://doi.org/10.1103/PhysRevB.94.104512)

I. INTRODUCTION

Recently, superconducting materials lacking in the inversion symmetry in their crystal structure were intensively investigated due to the possible exotic nature of their superconducting order parameter, which in the presence of a strong antisymmetric spin-orbit scattering, could in principle be a mixture of spin-singlet and spin-triplet components [1]. Moreover, under appropriate conditions, topologically nontrivial superconducting states can also be realized in these systems [2]. Experimental verification of both these possibilities is of extreme fundamental and applicative interest [3]. In addition, in the normal state antisymmetric spin-orbit scattering may be responsible for intriguing transport phenomena connecting charge and spin currents [1,4], on which the emergent field of spin orbitronics is based [5,6]. The presence of an unconventional superconducting pairing seems to be well established for some heavy fermion noncentrosymmetric superconductors (NCS) such as CePt_3Si [7] or CeRhSi_3 [8,9]. At the same time, superconductors with heavy transition elements may be more straightforward systems for exploring the consequences of inversion symmetry breaking. Indeed, in some cases exotic pairing was detected, as for instance in $\text{Li}_2\text{Pt}_3\text{B}$ [10,11], whereas for some other compounds, such as Re_6Zr [12,13] or BiPd [14–17], the results are still controversial. In particular, BiPd is especially interesting since for this material topologically nontrivial surface states were reported in the normal state [16]. Among transition-metal compounds, $\text{Nb}_x\text{Re}_{1-x}$ is a NCS which can be a possible candidate for having a nonconventional superconducting order parameter. Since Re is a heavy element, the effect of the antisymmetric spin-orbit scattering, the main ingredient affecting the pairing symmetry in these materials, is expected to be strong in the regime of low Nb percentage. The results observed on polycrystalline bulk samples were controversial [18–20], while the recent investigation [21] performed by combining point contact spectroscopy and heat capacity measurements on high quality $\text{Nb}_{0.18}\text{Re}_{0.82}$ single crystals [22] evidenced

the presence of two superconducting gaps. However, further experimental investigations are needed, since the employed measurement techniques did not provide enough insight to the symmetries of these two order parameters. Moreover, all the experimental studies on NCS focused so far on bulk samples, apart from preliminary attempts to produce $\text{Li}_2\text{Pt}_3\text{B}$ films [23], even if the possibility to produce NCS in the form of thin films is of extreme importance. First, the availability of NCS thin films may allow one to design dedicated transport experiments on heterostructures which are more sensitive to the spin symmetry of the superconducting order parameter [24,25]. Second, should the unique electronic properties of these materials be confirmed, any NCS-based device would employ them in a thin film form.

In this work noncentrosymmetric $\text{Nb}_x\text{Re}_{1-x}$ thin films were deposited and characterized and tunneling experiments were performed in order to determine the pairing symmetry of the superconducting order parameter in this system. The paper is organized as follows. Section II is devoted to the experimental results, namely, the samples fabrication (Sec. II A), the x-ray analysis (Sec. II B), and the electrical characterization both in the normal (Sec. II C) and in the superconducting (Sec. II D) state. In Sec. II E the conductance spectra measured on $\text{Al}/\text{Al}_2\text{O}_3/\text{NbRe}$ junctions as a function of the temperature are presented and analyzed. Finally, in Sec. III the issue of the triplet component of the superconducting order parameter is discussed and in Sec. IV the conclusions are reported.

II. EXPERIMENT

A. Sample fabrication

$\text{Nb}_x\text{Re}_{1-x}$ films of different thickness ($d = 3.5\text{--}200 \text{ nm}$) were grown on $\text{Si}(100)$ substrates by UHV dc diode magnetron sputtering from a $\text{Nb}_{0.20}\text{Re}_{0.80}$ 99.9% pure target. The deposition was performed keeping the substrate at room temperature in an Ar pressure of 3×10^{-3} mbar after obtaining a base pressure in the low 10^{-8} mbar regime. The deposition rate

was 0.32 nm/s, as measured by a quartz crystal monitor previously calibrated by low-angle x-ray reflectivity (XRR) measurements on a deliberately deposited thin film. The Nb concentration, as estimated by energy diffraction spectroscopy (EDS), was $x = 0.18$. Therefore the resulting $\text{Nb}_{0.18}\text{Re}_{0.82}$ (hereafter NbRe) films are close to the optimal Nb concentration in terms of superconducting transition temperature, T_c , as reported in the case of bulk samples [19]. The Al/ Al_2O_3 /NbRe junctions were realized as follows. A 60-nm-thick, 100- μm -wide Al strip was deposited on a Si/ SiO_2 substrate by rf magnetron sputtering and patterned by photolithography and lift-off. The Al deposition was performed keeping the substrate at room temperature in an Ar pressure of 3.2×10^{-3} mbar from a base pressure in the low 10^{-7} mbar regime. The deposition rate was 1.2 nm/s resulting in a roughness lower than 1 nm, as measured by atomic force microscopy. The insulating barrier was obtained by thermal oxidation of the Al strip in air at room temperature for several hours. In these conditions the thickness of grown Al_2O_3 is estimated to be saturated [26] at ~ 1.5 nm. Then a 100-nm-thick, 100- μm -wide NbRe counter electrode was deposited by dc sputtering as described previously, and patterned by photolithography and lift-off to cross the bottom Al/ Al_2O_3 strip. The resulting junction area is $A = (100 \times 100) \mu\text{m}^2$ with cross geometry that allows one to perform four contact measurements. With this method the resistance per area product of the junctions was in the range of $R \cdot A \sim \text{M}\Omega \mu\text{m}^2$. Such a large figure suggests that one is possibly concerned with reliable, pinhole-free tunnel barriers.

B. X-ray characterization

Low-angle reflectivity measurements, performed with a high resolution x-ray diffractometer with $\text{CuK}\alpha$ radiation, on a typical NbRe film of nominal thickness of 20 nm, are reported in Fig. 1 by open circles. The red line is the numerical simulation of the measured XRR profile, as obtained by using the software package GIXA using $d = 19$ nm and surface roughness of $\sigma = 1.0$ nm.

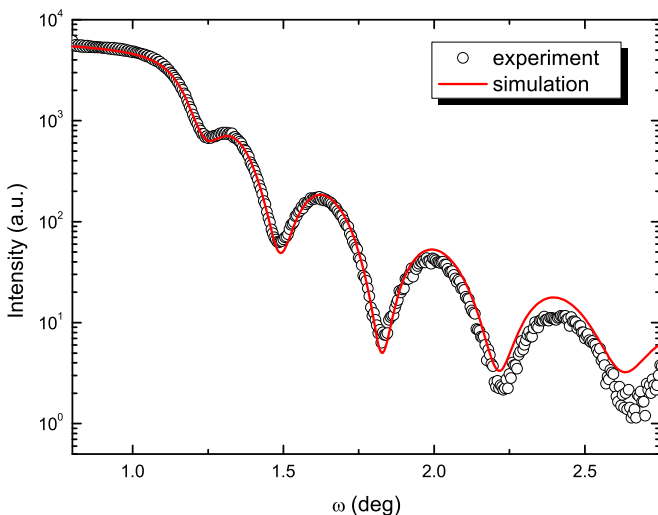


FIG. 1. Experimental (open circles) and simulated (red line) XRR profile for a NbRe thin film 19-nm thick.

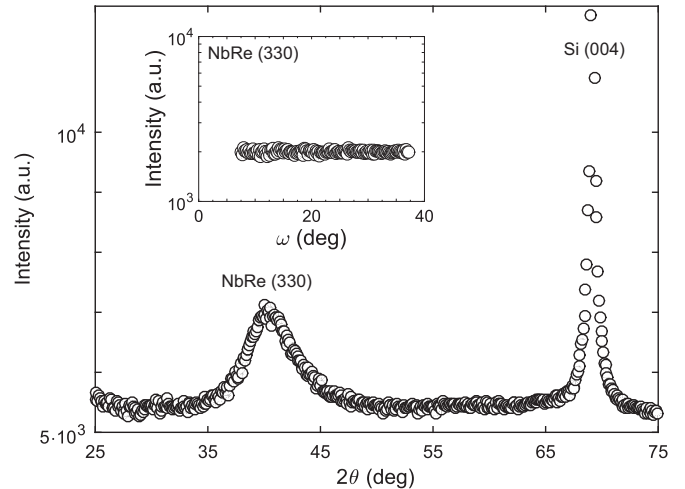


FIG. 2. XRD 2θ - ω scan of a NbRe film 200-nm thick. The inset shows the ω scan (rocking curve) of the (330) $\text{Nb}_{0.18}\text{Re}_{0.82}$ reflection.

The structural properties of the films were accurately determined by x-ray diffraction (XRD), performed with a four-circle Panalytical X'pert diffractometer with $\text{CuK}\alpha$ radiation, using a hybrid Ge(220) monochromator and a PIXcel 3D detector matrix.

The crystalline structure of the films was determined by symmetric 2θ - ω scans, as shown in Fig. 2 for a NbRe film with $d = 200$ nm. First of all, it should be noticed that no peaks corresponding to the single phases of Nb and Re are detected. Indeed, the primary peak, at $2\theta \approx 40^\circ$, can be consistently indexed as the (330) reflection, corresponding to the most intense peak expected for the noncentrosymmetric α -Mn cubic phase of NbRe [19,20]. From the peak position, a lattice parameter $a = 0.957$ nm is estimated, a value which is in good agreement with the expected one for the $\text{Nb}_{0.18}\text{Re}_{0.82}$ structure [18–20,27]. The large shape of this reflection indicates a small mean crystallite size within the film [28]. Moreover, the film is polycrystalline, as confirmed by the flat rocking curve measured on the (330) reflection (see inset of Fig. 2) [29]. This occurrence is an indication of a disordered structure, as also the large broadening of the primary peak in 2θ suggests. In this respect, efforts to optimize the quality of the NbRe films, by establishing a better matching between the films and the substrates, as well as by tuning the sputtering conditions (e.g., deposition temperature and rate) will be the object of future studies.

C. Normal state transport properties

Dealing with the first deposited NbRe films it is mandatory to perform a detailed electrical characterization of the samples also in the normal state. This analysis could in principle be useful also for future studies focusing on the nontrivial coupling between charge and spin degrees of freedom in the normal state. All the transport measurements were performed either in a liquid helium Dewar or in a ^4He cryostat, with the substrates glued with silver paint to a massive copper sample holder. The dc transport properties presented in this section were performed on unpatterned samples. A van der Pauw four leads configuration [30] was used to determine the

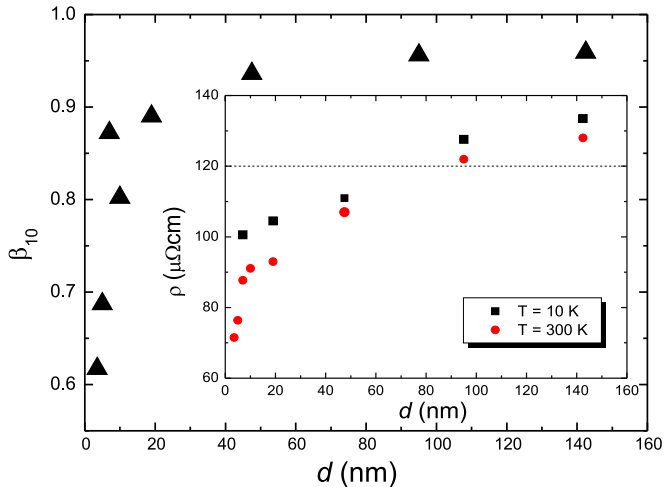


FIG. 3. Thickness dependence of the ratio β_{10} . Inset: electrical resistivities ρ_{300} (red circles) and ρ_{10} (black squares) as a function of the NbRe thickness. The dashed line indicates the value of the low temperature resistivity reported for Nb_{0.18}Re_{0.82} single crystals [22].

samples resistivity, ρ . A constant current, $I_b = 0.5$ mA, was applied to bias the samples. In the main panel of Fig. 3 the thickness dependence of the residual resistivity ratio, defined as the ratio between the value of the resistance at $T = 300$ K and $T = 10$ K ($\beta_{10} = R_{300}/R_{10}$), is reported. Here β_{10} , which quantifies the overall degree of purity and crystal perfection of a film, monotonically increases with the film thickness. This behavior, commonly reported for films of finite thickness, can be ascribed to the increase of the average grain size with d [31]. Its value stays below unity for the entire investigated thickness range, and tends to saturate to $\beta_{10} \approx 1$ for the thicker films. This result is typical of disordered superconductors, such as NbN [32,33]. It is worth reminding the reader that also in the case of NbRe single crystals [21] and polycrystalline samples [18] the values of β_{10} were relatively low, namely, $\beta_{10} \approx 1.14$ and 1.35, respectively. The comparison with the bulk value may suggest that the β_{10} values are not affected by structural issues. The thickness dependence of the resistivities, evaluated both at $T = 300$ K and $T = 10$ K (ρ_{300} and ρ_{10} , respectively), are reported in the inset of Fig. 3. Unexpectedly, both the resistivities increase with increasing the film thickness and it is also worth noticing that their saturation value is close to the one reported for NbRe single crystals [22] (dashed line). It is well known that conventional metallic superconductors usually present an opposite $\rho(d)$ dependence, which can be ascribed either to finite size effects [34], or to grain boundary scattering [31]. In particular, for both single Nb [35,36] and Re [37] thin films ρ decreases with increasing thickness. This point, together with the issue of the value of β_{10} will be investigated in the following, when also the values of the superconducting critical temperatures will be shown. Finally, following Ref. [38] the measured values of ρ_{10} , together with the value of the electron-phonon (e-ph) coupling constant [18], $\lambda_{e-ph} = 0.73$, seem to indicate that all the films are in the weak-coupling regime. This point will be further analyzed in the section devoted to tunneling experiments.

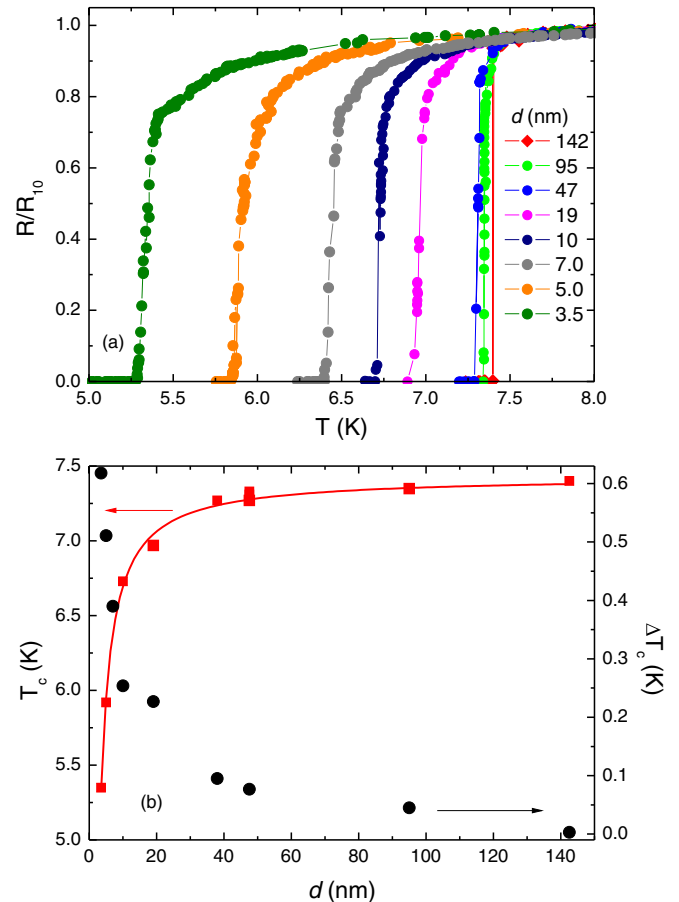


FIG. 4. (a) Normalized resistive transitions for some of the measured NbRe films. (b) Thickness dependence of the superconducting critical temperature T_c (left scale) and the amplitude of the resistive transitions, ΔT_c (right scale). The solid line is the fit to the $T_c(d)$ data according to the model in Ref. [39].

D. Superconducting properties

1. NbRe thin films

Following the deposition procedure described in Sec. II A, NbRe films with well established superconducting ordering were realized. As for the crystallographic properties, also the superconducting ones confirm that no spurious phases are present in the samples. The normalized resistive transitions, R/R_{10} , of a selection of unpatterned NbRe films are reported in Fig. 4(a). The superconducting critical temperature was defined as the temperature at which the resistance is half of the one measured at $T = 10$ K, $T_c \equiv T_c^{50\%}$. For the thickest measured film ($d = 142$ nm) $T_c = 7.40$ K, a value which is about one Kelvin lower than the one reported for single crystals with the same composition [21]. As can be better inferred from panel (b) of Fig. 4 (left scale), T_c is a monotonically increasing function of the film thickness, as for Nb [35,36] and Re [37], with a stronger dependence for $d \leq 20$ nm. The opposite dependence is found for the width of the resistive transitions, defined as $\Delta T_c = T_c^{90\%} - T_c^{10\%}$ [Fig. 4(b), right scale]. In fact, the transitions become sharper as d increases. Both of these last two dependencies indicate that the superconducting properties are strengthened as the film thickness is increased,

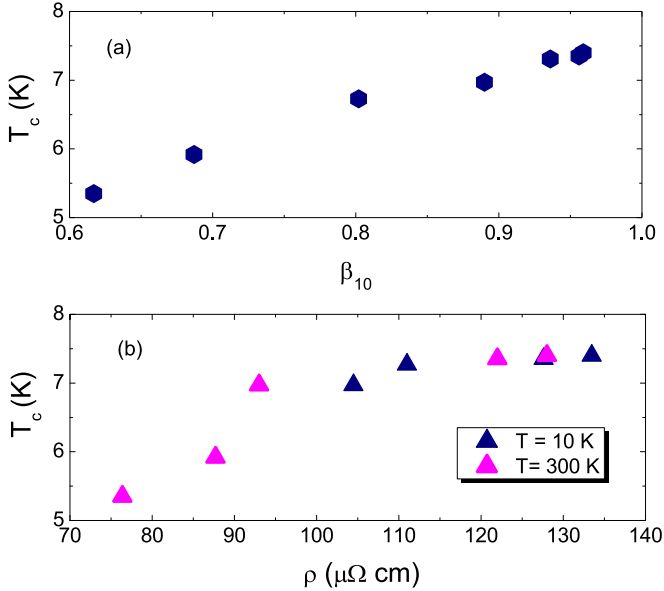


FIG. 5. Dependence of the critical temperature, T_c , on β_{10} (a) and ρ (b).

as commonly reported for conventional superconductors. In particular, it is interesting to point out that the thinnest film ($d = 3.5$ nm) still presents a noticeable critical temperature of 5.3 K. The decrease of T_c as a function of the film thickness is typically ascribed to the presence of the external surface of the film. This effect was studied in Ref. [39], where the following dependence was derived: $T_c = T_c^b(1 - d_{cr}/d)$. Here T_c^b is the critical temperature of the bulk superconductor and $d_{cr} = 2b/N(0)V$ is the critical thickness below which $T_c = 0$ [here b is the Thomas-Fermi screening length and $N(0)V$ is the bulk interaction potential]. The result of the fitting procedure on the $T_c(d)$ data using this last expression is reported in Fig. 4(b) as a solid line. Very good agreement is obtained with the parameters $T_c^b = 7.43$ K and $d_{cr} = 1.0$ nm. The extremely reduced value of the critical thickness is consistent with the small values of the superconducting coherence length, $\xi(0) = 4.3$ nm, reported for NbRe polycrystals [18] [the evaluation of $\xi(0)$ for the samples investigated here will be presented in the following]. It is well known, in fact, that the reduction of T_c with the thickness is more effective for $d \approx \xi$. In Fig. 5(a) the dependence of the critical temperature on β_{10} is shown. This behavior resembles that reported for Nb films [40], while it is opposite to the result obtained for Re films [37]. This point will be discussed below in terms of the position of the Fermi level in the density of states of these two materials. Finally, in Fig. 5(b) the dependence of the transition temperature on ρ is reported. Contrary to the results reported for both Nb [35,40] and Re [37], here T_c increases with increasing resistivity. Again, this behavior was reported in the literature for a variety of disordered films [41], such as irradiated Mo_3Ge [42]. In this last work the disorder induced by the radiation resulted in an enhancement of T_c , of the residual resistivity, and according to the authors, also of the value of the density of states in Mo_3Ge without reducing the electron-phonon interaction. Summarizing, the results reported in Fig. 5, as well as in the previous section,

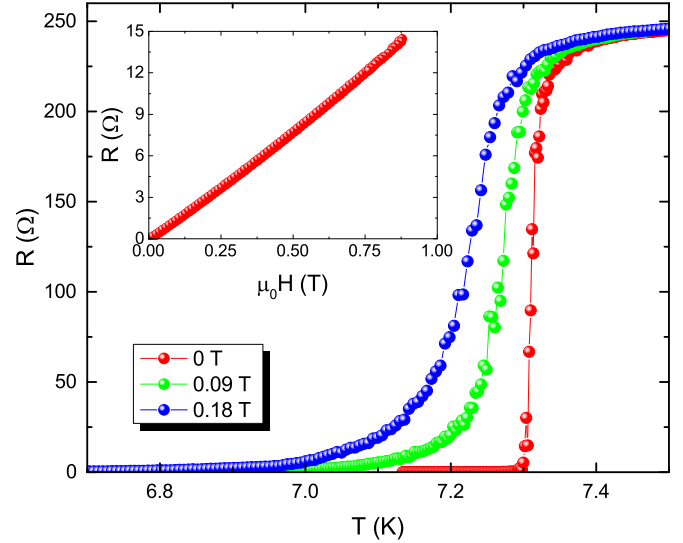


FIG. 6. Selection of resistive transition as a function of the temperature for different values of the magnetic field for a NbRe patterned film 60-nm thick. Inset: dependence of electrical resistance on the magnetic field, $R(\mu_0 H)$, at $T = 4.25$ K, in the low field region.

suggest that the transport properties are dominated by disorder. T_c increases or decreases with disorder depending on the shape of the density of states at the Fermi level $N(0)$. For weak-coupling superconductors, with low values of $N(0)$, and consequently low values of bulk T_c , such as Re, disorder determines an increase in $N(0)$. The opposite occurs for Nb, which has a peak at $N(0)$. In this case the smearing induced by disorder on the density of states, can produce a drop in T_c [42,43]. This observation further suggests that NbRe is in the weak-coupling regime.

2. NbRe bridges

In the following the electric transport measurements performed in the presence of a magnetic field are reported. For this purpose, the samples were structured into a Hall bar geometry of width $w = 100$ μm and distance between the voltage contacts $L = 1$ mm. In order to determine the value of the upper critical magnetic field at $T = 0$, $\mu_0 H_{c2}(0)$, resistance-vs-temperature, $R(T)$, measurements were performed at fixed values of the magnetic field close to T_c , with $I_b = 10$ μA . A selection of the $R(T)$ curves measured on a NbRe Hall bar with $d = 60$ nm is reported in the main panel of Fig. 6 for $\mu_0 H = 0, 0.09$, and 0.18 T. As in the case of bulk polycrystals, the width of the transitions increases by increasing the magnetic field [18]. By adopting the same resistance criterion reported above and extrapolating the linear dependence of $\mu_0 H_{c2}(T)$ down to $T = 0$, it follows that $\mu_0 H_{c2}(0) = 14.4 \pm 0.9$ T. With the assumption of a linear dependence of the perpendicular upper critical field, it is also possible to evaluate the superconducting coherence length, since $\mu_0 H_{c2}(0) = \Phi_0/2\pi\xi(0)^2$, where $\Phi_0 = 2.07 \times 10^{-15}$ Wb is the flux quantum [44]. This relation gives $\xi(0) = 4.8$ nm. From the value of $T_c = 7.3$ K and that of the low temperature resistivity $\rho_{10} = 148$ $\mu\Omega$ cm it is possible to extract the value of the magnetic penetration depth at zero temperature from the relation [45] $\lambda(0) = 1.05 \times 10^{-3}(\rho_{10}/T_c)^{0.5} = 472$ nm.

Therefore the Ginzburg-Landau parameter is $\kappa = \lambda/\xi = 98$. The knowledge of these microscopic parameters allows one to estimate the value of the lower critical field [44] $\mu_0 H_{c1}(0) = (\Phi_0/4\pi\lambda^2)\ln(\lambda/\xi) = 3.4 \times 10^{-3}$ T and of thermodynamic critical field [44] $\mu_0 H_c(0) = \kappa\sqrt{2}\mu_0 H_{c1}(0)/\ln\kappa = 0.10$ T, in reasonable agreement with the results on bulk polycrystals [18]. Moreover, from the slope of the $\mu_0 H_{c2}(T)$ curve the value of the quasiparticle diffusion coefficient D can be estimated [46], since $D = (4k_B/\pi e)(\mu_0 dH_{c2}/dT|_{T=T_c})^{-1} = 0.56 \times 10^{-4}$ m²/s, with $(\mu_0 dH_{c2}/dT|_{T=T_c}) = -2.0$ T/K. Finally, in the inset of Fig. 6 the low field region of the magnetoresistance curve [$R(\mu_0 H)$] measured on the same sample is shown. The curve, acquired at $T = 4.25$ K, with a bias current of $I_b = 10$ mA, was used for a further estimation of the value of $\mu_0 H_{c2}(0)$, as will be described in the following. $V(I)$ characteristics were also measured on the same samples with $d = 60$ nm. Electrical interference was minimized, filtering all cables with RC filters. Very low noise $V(I)$ characteristics as well as differential conductance-voltage curves, $G(V)$, were recorded using the 6221 current source/2182A nanovoltmeter combo from Keithley. In the upper inset of Fig. 7(a) a selection of the $V(I)$ characteristics at $T = 4.25$ K (corresponding to a reduced temperature $t = T/T_c = 0.58$) are shown. The curves were measured for different values of the magnetic field, from zero up to $\mu_0 H = 0.88$ T, which was applied perpendicularly to the sample surface. The main panel of Fig. 7(a) shows the dependence of the critical current density $J_c = I_c/(wd)$ on the magnetic field in a reduced field range (see discussion below). The critical current I_c was defined using a voltage criterion $V_c = 1$ μ V, which corresponds to an electric field criterion $E_c = 1$ nV/m. At zero magnetic field $J_c(0) = 8.3 \times 10^9$ A/m², a value which is comparable to the ones reported for Nb thin films [47]. From the analysis of the $J_c(\mu_0 H)$ dependence, information concerning the pinning strength of NbRe can be gained [48,49]. As shown in the lower inset of Fig. 7(a) by the dot-dashed line, in the low field regime, the critical current density decreases linearly with $\mu_0 H$, until J_c is reduced to half its value at zero field. This behavior is usually observed, together with a $\mu_0 H^{-1}$ dependence at higher fields, when the main pinning source is the bridge's edge [48]. Here a weaker field dependence is observed at higher fields, as can be inferred from the main panel of Fig. 7(a). The dashed line, which corresponds to the $\mu_0 H^{-1}$ dependence, lays below the experimental data in the entire investigated field range, while the solid one, which represents the $\mu_0 H^{-1/2}$ dependence, nicely reproduces the measured points up to $\mu_0 H = 0.05$ T, as reported for materials with stronger pinning, such as TaN [49]. An even weaker decrease is present for $\mu_0 H \geq 0.05$ T (for the sake of clearness, here the data were shown up to $\mu_0 H = 0.2$ T), which indicates that edge pinning is absent in the NbRe film in this field range. From the analysis of the $V(I)$ curves in the low voltage region, as shown in the inset of Fig. 7(b), it emerges that a linear voltage-current behavior, typical of a flux-flow regime, is always present even at very low current bias. It is worth commenting also on the sudden transition which follows the linear regime. Indeed, a clear jump to the normal state occurs at a current I^* , corresponding to a voltage V^* [see inset of Fig. 7(b)]. This point will be analyzed later. Now, since in the flux-flow regime [44] $R_f/R_n = H/H_{c2}(0)$, where R_f (R_n) is the flow (normal) resistance, from the linear

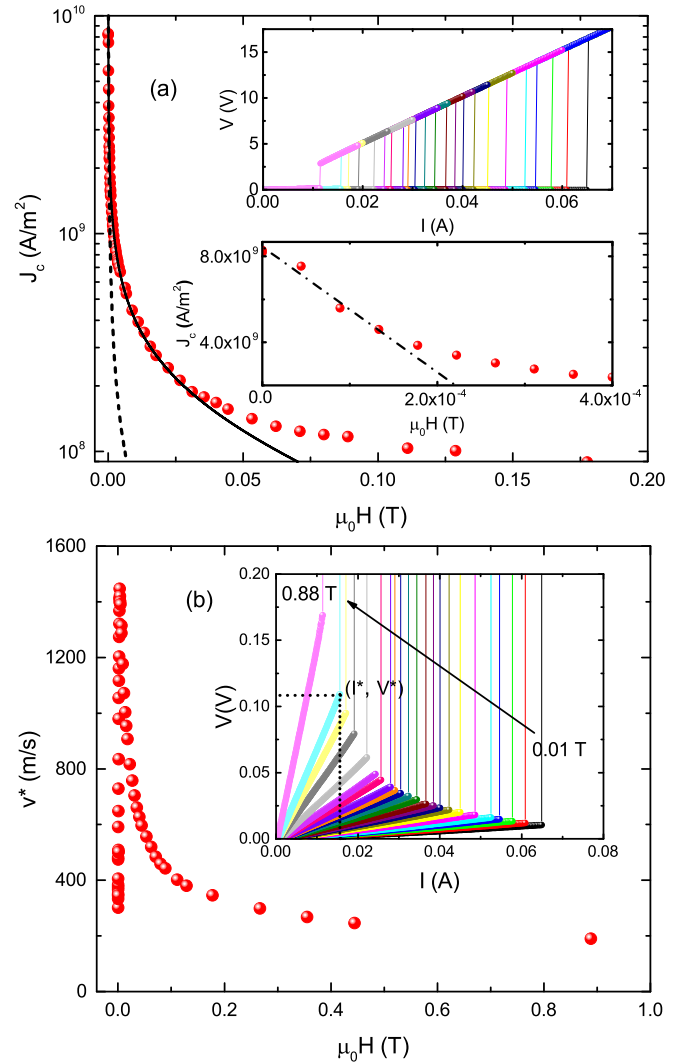


FIG. 7. (a) Dependence of the critical current density on the magnetic field, $J_c(\mu_0 H)$, for the same sample of Fig. 6 at $T = 4.25$ K. The dashed line shows the $\mu_0 H^{-1}$ field dependence, as expected when the dominant pinning mechanism is due to the bridge edge. By the continuous line the $\mu_0 H^{-1/2}$ behavior is reported. The upper inset shows some representative $V(I)$ curves for different values of the magnetic field, from zero up to $\mu_0 H = 0.88$ T. In the lower panel the low field regime of the $J_c(\mu_0 H)$ curve is reported, in order to highlight the linear field dependence (dot-dashed line), also due to edge pinning. (b) Dependence of the critical velocity, v^* , as a function of the magnetic field, $\mu_0 H$, at $T = 4.25$ K. Inset: $V(I)$ curves shown on a small voltage range at $T = 4.25$ K for increasing magnetic field (as indicated by the arrow) from $\mu_0 H = 0.01$ T to $\mu_0 H^{\max} = 0.88$ T. The definition of both the current I^* and the voltage V^* are indicated for the sake of clearness.

fit of the $V(I)$ curves it is possible to estimate the value of the upper critical magnetic field at $T = 0$ and to compare it with the one extracted from the $R(T)$ curves. It results that $\mu_0 H_{c2}^{V(I)} = 14.4 \pm 0.3$ T. Finally, the same analyses were also performed on the $R(\mu_0 H)$ curve reported in the inset of Fig. 6. From a linear fit of the low field region, according to the same expression valid in the flux-flow regime, it results that

TABLE I. Values of the parameters which characterize the 60-nm-thick NbRe patterned film, as extracted from the $V(I)$, $R(H)$, and $R(T)$ curves.

Parameters	Estimated values
T_c	(7.3 ± 0.1) K
ρ_{10}	$148 \mu\Omega \text{ cm}$
$\mu_0 H_{c1}(0)$	3.4×10^{-3} T
$\mu_0 H_{c2}(0)$	(14.4 ± 0.9) T
$\mu_0(dH_{c2}/dT)_{T=T_c}$	(-2.0 ± 0.1) T/K
$\mu_0 H_c(0)$	0.10 T
$\xi(0)$	4.8 nm
$\lambda(0)$	472 nm

$\mu_0 H_{c2}^{RH}(0) = 15.0 \pm 0.3$ T. It follows that all the estimations of $\mu_0 H_{c2}(0)$ are in agreement within the experimental error.

Returning to the issue of the jump in the $V(I)$ curves [see inset of Fig. 7(b)], it is well known that the voltage V^* corresponding to the value of the current I^* , where the jumps are detected, can be interpreted as the Larkin and Ovchinnikov flux-flow instability at the velocity v^* . Following Ref. [50], it is $V^* = \mu_0 v^* H L$ and the critical velocity can be expressed as $v^* = D^{1/2} [14\zeta(3)]^{1/4} (1-t)^{1/4} / \pi \tau_E^{1/2}$, which means that from measuring the critical voltage V^* it is possible to estimate the values of the quasiparticle relaxation times, τ_E . Here $\zeta(x)$ is the Riemann zeta function and D is the quasiparticle diffusion coefficient. In Fig. 7(b) the dependence of the critical velocity on the magnetic field at $T = 4.25$ K is reported. At very low fields a peak is present, as already observed for different superconducting materials both in the nonmesoscopic [51], as well as in the mesoscopic regime [52]. From the values of v^* , it follows that the values of the relaxation time at $t = 0.58$ span from $\tau_E^{\min} = 2.3 \times 10^{-11}$ s at $\mu_0 H = 0.003$ T (corresponding to the peak in the field dependence of v^*), to $\tau_E^{\max} = 1.3 \times 10^{-9}$ s at $\mu_0 H = 0.88$ T. By comparing these values with those reported in the literature [53], it seems that in NbRe the energy relaxation processes are faster than in Nb and of the same order of magnitude as in NbN, which, due to the extremely reduced characteristic e-ph coupling time [54], is characterized by the extremely reduced value of τ_E . This result could also be ascribed to the disorder present in the sample, since it can cause an appreciable reduction of the quasiparticles lifetimes [53,55]. In Table I all the parameters estimated for the 60-nm-thick patterned sample are summarized.

E. Tunneling spectroscopy

Useful information on the order parameter of a superconductor can be extracted by analysis of differential conductance curves, $G(V)$, of tunnel junctions [44,56] or point contacts within the model of Blonder, Tinkham, and Klapwijk (BTK) [57] and its extensions [58]. Here the tunnel junction method, which is more suited for thin films, was chosen. In the fabricated N-I-S tunnel junctions, the superconductor (S) is NbRe, the normal metal (N) is Al, and the thin insulator (I) is Al_2O_3 , the reliable native oxide of Al. A sketch of the junction, which illustrates the four contact measurement configuration,

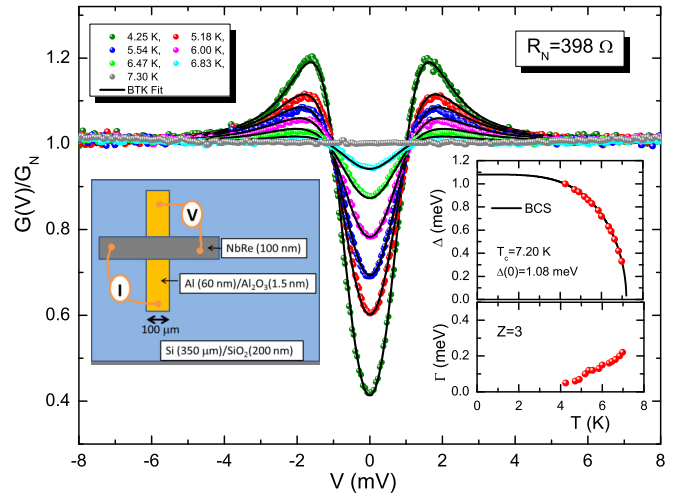


FIG. 8. Normalized conductance spectra (points) of a tunnel junction are fitted with the BTK model (lines). The geometry of the measured tunnel junction is shown in the left inset. The energy gap $\Delta(T)$ and the broadening parameter $\Gamma(T)$ as estimated from the fit are shown in the right inset. The estimated $\Delta(T)$ (points) can be nicely fitted with the BCS behavior (line).

is shown in the left inset of Fig. 8. From the analysis of several junctions similar results were obtained. For the representative junction reported here, the normal state resistance at $T = 7.5$ K was $R_N \approx 398 \Omega$ ($RA \approx 4 \text{ M}\Omega \mu\text{m}^2$) and the critical temperature of the NbRe counterelectrode was $T_c \approx 7.20$ K. A representative set of the $G(V)$ curve of this junction at several temperatures is shown in the main panel of Fig. 8. In order to allow a direct comparison with theory, the conductance curves are normalized to the conductance in the normal state at 7.5 K, $G_N = 1/R_N$. At first glance, the conductance spectra suggest that a standard BCS [44,59] order parameter is possibly exhibited by the polycrystalline NbRe films. In fact, the experimental spectra can be satisfactorily fitted with the BTK model [57], which assumes a single isotropic order parameter with s -wave symmetry. Some representative fitting curves are plotted in the main panel of Fig. 8. Even though a reasonable fit was achieved also within the simple version of the model, a more satisfactory agreement was achieved applying the BTK model [58,60], which includes the broadening parameter Γ introduced by Dynes *et al.* [61]. As usual [58,60], in the fits a temperature-independent barrier strength [57] parameter Z , a temperature-dependent superconducting gap amplitude $\Delta(T)$, and a temperature-dependent broadening parameter $\Gamma(T)$ were assumed. The best fits were achieved with $Z = 3$, a result which confirms that a tunnel regime is realized. In agreement with the finding of Dynes *et al.* [61], the broadening parameter is found to be reasonably small at the lowest temperature [$\Gamma(4.25 \text{ K}) = 0.02$ meV] and to increase with temperature. This value is consistent with the estimate of the relaxation time evaluated in the previous section. Indeed, $\tau_E = \hbar/\Gamma$, therefore at $T = 4.25$ K and $H = 0$ it is $\tau_E = 3.3 \times 10^{-11}$ s, in reasonable agreement with the value resulting from the $V(I)$ analysis for τ_E^{\min} . The values of $\Delta(T)$ and $\Gamma(T)$ extracted from the fits of all the measured conductance curves are shown in the right inset of Fig. 8. The $\Delta(T)$ is found to be well fitted with

the BCS behavior [44,59] using $\Delta(0)$ and $T_c^{(\text{fit})}$ as parameters. The best fit is achieved with $\Delta(0) = 1.08 \pm 0.02$ meV and $T_c^{(\text{fit})} = 7.20 \pm 0.01$ K, i.e., the critical temperature of the used NbRe counterelectrode, a value which is in agreement with the T_c of a plane NbRe film of the same thickness [see Fig. 4(b)]. A comparison of the estimated value of the energy gap at zero $\Delta(0)$ with the one expected from BCS relation [44] $\Delta_{\text{BCS}}(0) = 1.76k_B T_c \approx 1.09$ meV confirms that the NbRe films under investigation are weak-coupling [44] superconductors.

III. DISCUSSION

Having performed a deep characterization of the NbRe films deposited, it is worth comparing the obtained results with those reported in literature for bulk samples, both in polycrystalline [18–20] and in single crystal [21] form. Concerning the microscopical parameters extracted from the transport measurements, apart from the values of the critical temperature at the saturation as a function of the thickness, which is depressed of about 1 K with respect to the bulk value, there is general agreement between the values of the physical parameters extracted for the films and the bulk. The low temperature resistivity of the thickest film $\rho_{10} = 133 \mu\Omega \text{ cm}$ is slightly lower than the one reported for single crystals [22] and for polycrystals of Ref. [19], but higher than the one estimated on other polycrystalline samples of Ref. [18]. The low residual resistivity ratio found here is compatible with the values of β_{10} of single- [21] and poly- [18] crystals, namely, $\beta_{10} = 1.14$ and $\beta_{10} = 1.35$, respectively. The values of the coherence length $\xi(0) = 4.8$ nm are in good agreement with the figures reported in previous works for bulk NbRe [18,19]. On the contrary, as expected for a film, the penetration depth $\lambda(0) = 472$ nm is larger compared to the bulk. A general accordance holds for the values of the critical fields. Particularly interesting is, in this respect, the high values estimated for the perpendicular upper critical field at zero temperature (between 14 and 15 T), since this result is generally interpreted as a possible fingerprint of the presence of a triplet component of the order parameter. Indeed, as found for some polycrystalline samples [18,19], here $\mu_0 H_{c2}(0)$ is close to the Pauli limiting field, which can be obtained from the tunneling measurements as $\mu_0 H_{\text{Pauli}} = \Delta(0)/(\mu_B \sqrt{2}) = 13$ T. The temperature-dependent tunneling spectra on the first junctions based on NbRe films are fully compatible with a BCS single gap order parameter. A different result was recently obtained performing soft point contact spectroscopy on NbRe single crystals [21], where a two-gap structure described by a two-band model with isotropic spin-singlet pairing symmetry was observed. This controversial result may possibly originate from the lack of directionality in the tunnel experiment. Indeed, for both point contact and tunnel experiments, it is highly desirable to perform direction-controlled spectroscopy

in order to control the direction of the current injection with respect to the crystallographic axes [62]. Unfortunately, this condition was not fulfilled here, since, as revealed by the XRD data, the films are not epitaxial. Indeed, an unconventional pairing, if present, could be hindered by an averaging over the different crystallographic orientation. Moreover, as reported in Ref. [63], the presence of defects or impurities could affect the unconventional pairing. Therefore, as for the bulk samples the debated results obtained on polycrystals [18–20] stimulated the investigation of single crystals; similarly here, the investigation of epitaxial films would cast a new light on the nature of the pairing symmetry in NbRe. Indeed, fine tuning of the deposition conditions is in progress in order to enhance the film quality and, consequently, to perform more reliable direction-controlled experiments to access the wave symmetry of the superconducting order parameter, using both single films as well as heterostructures [24,25].

IV. CONCLUSIONS

In conclusion, superconducting Nb_{0.18}Re_{0.82} films with the desired crystallographic ordering were successfully deposited on Si(100) substrates. The samples were deeply characterized, both structurally and electrically. XRD measurements show that the films are polycrystalline, with a preferred $(nn0)$ growth which is compatible with the noncentrosymmetric α -Mn structure expected for this composition [27]. The transport properties seem to be strongly influenced by disorder; nevertheless, the films exhibit well established superconducting properties. Attention was devoted to the investigation of the nature of the superconducting order parameter. In this respect the values of $\mu_0 H_{c2}(0)$ comparable to $\mu_0 H_{\text{Pauli}}$ could in principle support the possible presence of an unconventional pairing [18,19]. On the other hand, tunnel conductance spectra, measured on high quality Al/Al₂O₃/NbRe tunnel junctions realized on NCS materials, can be described by a single gap s -wave model, providing strong evidence for conventional superconducting pairing. Finally, from the estimated value of the superconducting order parameter at $T = 0$, it follows that the ratio $\Delta(0) = 1.76k_B T_c$ indicates a weak electron-phonon coupling. Deeper insight is expected from tunneling experiments on epitaxial films. Moreover, the successful realization of reliable NbRe-based hybrid systems opens the possibility for further studies devoted to both unveiling the issue of the nature of the superconducting order parameter and taking advantage of the antisymmetric spin-orbit scattering in the normal state.

ACKNOWLEDGMENTS

The authors gratefully acknowledge Dr. R. Fittipaldi for the EDS analysis, Professor J. Aarts for the XRR measurements, and Dr. M. Cuoco for useful discussions.

-
- [1] E. Bauer and M. Sigrist, *Non-Centrosymmetric Superconductors: Introduction and Overview* (Springer, London, 2012).
 [2] M. Sato and S. Fujimoto, *Phys. Rev. B* **79**, 094504 (2009).
 [3] M. Eschrig, *Rep. Prog. Phys.* **78**, 104501 (2015).

- [4] A. Manchon, H. C. Koo, J. Nitta, S. M. Frolov, and R. A. Duine, *Nat. Mater.* **14**, 871 (2015).
 [5] A. Hoffmann and S. D. Bader, *Phys. Rev. Appl.* **4**, 047001 (2015).
 [6] T. Kuschel and G. Reiss, *Nat. Nanotechnol.* **10**, 22 (2015).

- [7] E. Bauer, G. Hilscher, H. Michor, Ch. Paul, E. W. Scheidt, A. Griбанov, Yu. Seropegin, H. Noël, M. Sigrist, and P. Rogl, *Phys. Rev. Lett.* **92**, 027003 (2004).
- [8] N. Kimura, K. Ito, K. Saitoh, Y. Umeda, H. Aoki, and T. Terashima, *Phys. Rev. Lett.* **95**, 247004 (2005).
- [9] N. Kimura, K. Ito, H. Aoki, S. Uji, and T. Terashima, *Phys. Rev. Lett.* **98**, 197001 (2007).
- [10] H. Q. Yuan, D. F. Agterberg, N. Hayashi, P. Badica, D. Vandervelde, K. Togano, M. Sigrist, and M. B. Salamon, *Phys. Rev. Lett.* **97**, 017006 (2006).
- [11] M. Nishiyama, Y. Inada, and Guo-qing Zheng, *Phys. Rev. Lett.* **98**, 047002 (2007).
- [12] R. P. Singh, A. D. Hillier, B. Mazidian, J. Quintanilla, J. F. Annett, D. McK. Paul, G. Balakrishnan, and M. R. Lees, *Phys. Rev. Lett.* **112**, 107002 (2014).
- [13] M. A. Khan, A. B. Karki, J. C. Prestigiacomo, T. Samanta, D. Browne, S. Stadler, I. Vekhter, P. W. Adams, A. Pandey, D. P. Young, R. Prozorov, S. Teknowijoyo, K. Cho, and D. E. Graf, *arXiv:1603.07297*.
- [14] M. Mondal, B. Joshi, S. Kumar, A. Kamlapure, S. C. Ganguli, A. Thamizhavel, S. S. Mandal, S. Ramakrishnan, and P. Raychaudhuri, *Phys. Rev. B* **86**, 094520 (2012).
- [15] L. Jiao, J. L. Zhang, Y. Chen, Z. F. Weng, Y. M. Shao, J. Y. Feng, X. Lu, B. Joshi, A. Thamizhavel, S. Ramakrishnan, and H. Q. Yuan, *Phys. Rev. B* **89**, 060507(R) (2014).
- [16] Z. Sun, M. Enayat, A. Maldonado, C. Lithgow, E. Yelland, D. C. Peets, A. Yaresko, A. P. Schnyder, and P. Wahl, *Nat. Commun.* **6**, 6633 (2015).
- [17] D. C. Peets, A. Maldonado, M. Enayat, Z. Sun, P. Wahl, and A. P. Schnyder, *Phys. Rev. B* **93**, 174504 (2016).
- [18] A. B. Karki, Y. M. Xiong, N. Haldolaarachchige, S. Stadler, I. Vekhter, P. W. Adams, D. P. Young, W. A. Phelan, and J. Y. Chan, *Phys. Rev. B* **83**, 144525 (2011).
- [19] J. Chen, L. Jiao, J. L. Zhang, Y. Chen, L. Yang, M. Nicklas, F. Steglich, and H. Q. Yuan, *Phys. Rev. B* **88**, 144510 (2013).
- [20] C. S. Lue, T. H. Su, H. F. Liu, and B.-L. Young, *Phys. Rev. B* **84**, 052509 (2011).
- [21] C. Cirillo, R. Fittipaldi, M. Smidman, G. Carapella, C. Attanasio, A. Vecchione, R. P. Singh, M. R. Lees, G. Balakrishnan, and M. Cuoco, *Phys. Rev. B* **91**, 134508 (2015).
- [22] R. P. Singh, M. Smidman, M. R. Lees, D. McK Paul, and G. Balakrishnan, *J. Cryst. Growth* **361**, 129 (2012).
- [23] P. Badica and G. Jakob, *Physica C* **470**, S655 (2010).
- [24] H. Zhang, J. Wang, and Jun-Feng Liu, *Appl. Phys. Lett.* **108**, 102601 (2016).
- [25] A. Romano, P. Gentile, C. Noce, I. Vekhter, and M. Cuoco, *Phys. Rev. B* **93**, 014510 (2016).
- [26] E. Cimpoiasu, S. K. Tolpygo, X. Liu, N. Simonian, J. E. Lukens, K. K. Likharev, R. F. Klie, and Y. Zhu, *J. Appl. Phys.* **96**, 1088 (2004).
- [27] A. G. Knapton, *J. Less-Common Met.* **1**, 480 (1959).
- [28] R. Banerjee, E. A. Sperling, G. B. Thompson, H. L. Fraser, S. Bose, and P. Ayyub, *Appl. Phys. Lett.* **82**, 4250 (2003).
- [29] R. E. Treece, J. S. Horwitz, J. H. Claassen, and D. B. Chrisey, *Appl. Phys. Lett.* **65**, 2860 (1994).
- [30] L. J. van der Pauw, *Philips Res. Rep.* **13**, 1 (1958).
- [31] A. Andreone, A. Cassinese, M. Iavarone, R. Vaglio, I. I. Kulik, and V. Palmieri, *Phys. Rev. B* **52**, 4473 (1995).
- [32] A. Nigro, G. Nobile, M. G. Rubino, and R. Vaglio, *Phys. Rev. B* **37**, 3970 (1988).
- [33] F. Marsili, A. Gaggero, L. H. Li, A. Surrente, R. Leoni, F. Levy, and A. Fiore, *Supercond. Sci. Technol.* **22**, 095013 (2009).
- [34] K. Fuchs, *Proc. Cambridge Philos. Soc.* **34**, 100 (1938); E. H. Sondheimer, *Adv. Phys.* **1**, 1 (1952).
- [35] M. S. M. Minhaj, S. Meepagala, J. T. Chen, and L. E. Wenger, *Phys. Rev. B* **49**, 15235 (1994).
- [36] C. Cirillo, A. Rusanov, C. Bell, and J. Aarts, *Phys. Rev. B* **75**, 174510 (2007).
- [37] A. Ul Haq and O. Meyer, *Thin Solid Films* **94**, 119 (1982).
- [38] M. Gurvitch, *Phys. Rev. Lett.* **56**, 647 (1986).
- [39] J. Simonin, *Phys. Rev. B* **33**, 7830 (1986).
- [40] C. Camerlingo, P. Scardi, C. Tosello, and R. Vaglio, *Phys. Rev. B* **31**, 3121 (1985).
- [41] J. W. Garland, K. H. Bennemann, and F. M. Mueller, *Phys. Rev. Lett.* **21**, 1315 (1968).
- [42] M. Gurvitch, A. K. Ghosh, B. L. Gyorffy, H. Lutz, O. F. Kammerer, J. S. Rosner, and M. Strongin, *Phys. Rev. Lett.* **41**, 1616 (1978).
- [43] J. E. Crow, M. Strongin, R. S. Thompson, and O. F. Kammerer, *Phys. Lett. A* **30**, 161 (1969).
- [44] M. Tinkham, *Introduction to Superconductivity* (McGraw-Hill, Singapore, 1996).
- [45] P. H. Kes and C. C. Tsuei, *Phys. Rev. B* **28**, 5126 (1983).
- [46] J. Guimpel, M. E. de la Cruz, F. de la Cruz, H. J. Fink, O. Laborde, and J. C. Villegier, *J. Low Temp. Phys.* **63**, 151 (1986).
- [47] P. Sabatino, C. Cirillo, G. Carapella, M. Trezza, and C. Attanasio, *J. Appl. Phys.* **108**, 053906 (2010).
- [48] B. L. T. Plourde, D. J. Van Harlingen, D. Yu. Vodolazov, R. Besseling, M. B. S. Hesselberth, and P. H. Kes, *Phys. Rev. B* **64**, 014503 (2001).
- [49] K. Ilin, D. Henrich, Y. Luck, Y. Liang, M. Siegel, and D. Yu. Vodolazov, *Phys. Rev. B* **89**, 184511 (2014).
- [50] W. Klein, R. P. Huebener, S. Gauss, and J. Parisi, *J. Low Temp. Phys.* **61**, 413 (1985).
- [51] G. Grimaldi, A. Leo, C. Cirillo, A. Casaburi, R. Cristiano, C. Attanasio, A. Nigro, S. Pace, and R. P. Huebener, *J. Supercond. Nov. Magn.* **24**, 81 (2011).
- [52] G. Grimaldi, A. Leo, P. Sabatino, G. Carapella, A. Nigro, S. Pace, V. V. Moshchalkov, and A. V. Silhanek, *Phys. Rev. B* **92**, 024513 (2015).
- [53] C. Attanasio and C. Cirillo, *J. Phys.: Condens. Matter* **24**, 083201 (2012).
- [54] L. Parlato, R. Latempa, G. Peluso, G. P. Pepe, R. Cristiano, and R. Sobolewski, *Supercond. Sci. Technol.* **18**, 1244 (2005).
- [55] C. Peroz and C. Villard, *Phys. Rev. B* **72**, 014515 (2005).
- [56] I. Giaever, *Phys. Rev. Lett.* **5**, 464 (1960).
- [57] G. E. Blonder, M. Tinkham, and T. M. Klapwijk, *Phys. Rev. B* **25**, 4515 (1982).
- [58] D. Daghero and R. S. Gonnelli, *Supercond. Sci. Technol.* **23**, 043001 (2010).
- [59] J. Bardeen, L. N. Cooper, and J. R. Schrieffer, *Phys. Rev.* **108**, 1175 (1957).
- [60] A. Plecenik, M. Grajcar, Š. Beňačka, P. Seidel, and A. Pfuch, *Phys. Rev. B* **49**, 10016 (1994).
- [61] R. C. Dynes, V. Narayanamurti, and J. P. Garno, *Phys. Rev. Lett.* **41**, 1509 (1978).
- [62] D. Daghero, M. Tortello, P. Pecchio, V. A. Stepanov, and R. S. Gonnelli, *Low Temp. Phys.* **39**, 199 (2013).
- [63] V. P. Mineev and K. V. Samokhin, *Phys. Rev. B* **75**, 184529 (2007).